RESEARCH ARTICLES

HGT

Dose-Escalation Study of Systemically Delivered rAAVrh74.MHCK7.micro-dystrophin in the *mdx* Mouse Model of Duchenne Muscular Dystrophy

Rachael A. Potter,[1,2] Danielle A. Griffin,[1,2] Kristin N. Heller,[2] Ellyn L. Peterson,[1,2] Emma K. Clark,[2] Jerry R. Mendell,[2,3] and Louise R. Rodino-Klapac[1–3]

[1]*Sarepta Therapeutics, Inc., Cambridge, Massachusetts, USA.*
[2]*Center for Gene Therapy, The Research Institute at Nationwide Children's Hospital, Columbus, Ohio, USA.*
[3]*Department of Pediatrics and Neurology, The Ohio State University, Columbus, Ohio, USA.*

Duchenne muscular dystrophy (DMD) is a rare, X-linked, fatal, degenerative neuromuscular disease caused by mutations in the *DMD* gene. More than 2,000 mutations of the *DMD* gene are responsible for progressive loss of muscle strength, loss of ambulation, and generally respiratory and cardiac failure by age 30. Recently, gene transfer therapy has received widespread interest as a disease-modifying treatment for all patients with DMD. We designed an adeno-associated virus vector (rAAVrh74) containing a codon-optimized human micro-dystrophin transgene driven by a skeletal and cardiac muscle-specific promoter, MHCK7. To test the efficacy of rAAVrh74.MHCK7.micro-dystrophin, we evaluated systemic injections in *mdx* (dystrophin-null) mice at low (2×10^{12} vector genome [vg] total dose, 8×10^{13} vg/kg), intermediate (6×10^{12} vg total dose, 2×10^{14} vg/kg), and high doses (1.2×10^{13} vg total dose, 6×10^{14} vg/kg). Three months posttreatment, specific force increased in the diaphragm (DIA) and tibialis anterior muscle, with intermediate and high doses eliciting force outputs at wild-type (WT) levels. Histological improvement included reductions in fibrosis and normalization of myofiber size, specifically in the DIA, where results for low and intermediate doses were not significantly different from the WT. Significant reduction in central nucleation was also observed, although complete normalization to WT was not seen. No vector-associated toxicity was reported either by clinical or organ-specific laboratory assessments or following formal histopathology. The findings in this preclinical study provided proof of principle for safety and efficacy of systemic delivery of rAAVrh74.MHCK7.micro-dystrophin at high vector titers, supporting initiation of a Phase I/II safety study in boys with DMD.

Keywords: Duchenne muscular dystrophy, AAV, micro-dystrophin, dose-escalation, gene therapy, rAAVrh74.MHCK7.micro-dystrophin, *mdx* mouse model

INTRODUCTION

DUCHENNE MUSCULAR DYSTROPHY (DMD) is a rare, X-linked, fatal, degenerative neuromuscular disease that occurs in ~1 in every 3,500 to 5,000 males born worldwide.[1–4] DMD and Becker muscular dystrophy (BMD) affect skeletal and cardiac muscle due to mutations in the 2.4 Mb dystrophin gene (*DMD*). Dystrophin is a 427 kDa cytoskeletal protein required for muscle fiber stability. Specifically, dystrophin links the sarcomere and the extracellular matrix. Loss of the protein results in destabilization of the dystrophin-associated protein complex (DAPC), repeated turnover of the muscle, satellite cell depletion, and replacement of fibers by fat and fibrosis. The most frequent mutations (65%) found in patients are deletions of one or more exons of the *DMD* gene, leading to shortened forms of nonfunctional dystrophin protein that undergo degradation.[5] Patients with DMD are characterized by progressive muscle weakness affecting skeletal and respiratory muscle and loss of ambulation typically by age 12, and generally death by age 30.[6]

Corticosteroids are currently the standard-of-care treatment for most patients to modify symptoms.[7] However, while corticosteroids have shown benefit in delaying disease progression, long-term treatment is limited as it is

*Correspondence: Dr. Louise R. Rodino-Klapac, Sarepta Therapeutics, Inc., 215 First Street, Cambridge, MA, 02142, USA. E-mail: lrodinoklapac@sarepta.com

associated with serious adverse effects such as bone fracture, infection, and gastrointestinal bleeding.[8] Moreover, once decline occurs, disease progression remains fatal as dilated cardiomyopathy and respiratory failure are often the major cause of premature death.[6] Eteplirsen is the first disease-modifying treatment (phosphorodiamidate morpholino oligomer) approved in the United States for DMD in patients with confirmed *DMD* mutations amenable to exon 51 skipping.[9–11] Eteplirsen has been shown to produce functional dystrophin protein and slow the decline in ambulatory and pulmonary function after long-term use.[9–12] Golodirsen was the first treatment approved by the U.S. Food and Drug Administration for DMD patients amenable to exon 53 skipping,[13] and a second antisense oligonucleotide has been approved for the same group of patients.[14] Recently there has been a significant focus on developing gene therapy approaches for DMD with the potential to become a disease-modifying treatment for all patients with DMD following single gene delivery.

Adeno-associated virus (AAV) systemic gene transfer therapy offers the possibility to ameliorate disease progression and normalize the muscle environment through restoration of dystrophin expression in cardiac and skeletal muscle. However, due to the enormous size of the dystrophin gene and the packaging limitation of AAV ($\sim$5 kb), entire gene transfer is not feasible. Thus, investigators have developed micro-dystrophin genes that produce shortened functional variants of micro-dystrophin protein and demonstrated amelioration of muscle pathology and cardiomyopathy in various preclinical models.[15–20]

More than 30 different configurations of micro-dystrophin have been developed based upon the genotypes of patients with milder forms of DMD/BMD and preclinical structure–function studies.[21] Dystrophin is composed of four major domains: an N-terminus that contains an actin binding domain, a central rod domain of 24 spectrin repeats (R) that is flanked and interspersed with 4 hinge (H) subdomains, a cysteine-rich domain, and a C-terminal domain.[22–24] The N-terminus and cysteine-rich domain are thought to be essential, as these contain an actin binding site[22] and the binding domain for β-dystroglycan,[25,26] respectively. In contrast, the C-terminus does not appear to be essential for muscle function or DAPC assembly.[23] The central rod domain is the largest and plays an important role in conferring protection and flexibility.[24,27] However, only a few spectrin repeats and hinges have been demonstrated to have functional relevance.[27,28] For example, spectrin repeats R2-3 have been shown to be necessary for optimized resistance to eccentric force loss,[28] and early structural studies have demonstrated that R1-3 may interact with the lipid membrane.[29,30] We have designed a micro-dystrophin transgene that would promote optimized functional efficacy upon delivery.

In addition to the micro-dystrophin transgene sequence, the efficacy and safety of AAV micro-dystrophin gene therapy are also dictated by the promoter sequence. Therefore, to maximize gene expression in cardiac and skeletal muscle, the cassette used for this study includes a skeletal and cardiac muscle-specific promoter, MHCK7, which provides assurance of safety and avoidance of off-target effects.[31,32] This promoter includes an α-myosin heavy chain complex (α-MHC) enhancer that leads to high levels of expression in cardiomyocytes and increased dystrophin expression in skeletal muscle versus MCK or CK7.[32–34] In the present study, a dose-escalation study design was utilized to evaluate safety and efficacy in the *mdx* mouse model of DMD. This report provides proof of principle for the efficacy and safety of systemic delivery of rAAVrh74.MHCK7.micro-dystrophin vector in an *mdx* mouse model of DMD at 3 and 6 months post-transgene delivery and supports initiation of a Phase I/II safety study in boys with DMD.

MATERIALS AND METHODS

Animal models

Dystrophin-deficient mouse strain. All procedures were approved by The Research Institute at Nationwide Children's Hospital Institutional Animal Care and Use Committee (protocol AR08-00009; AR06-00054). Stocks of C57BL/6 and C57BL/10ScSn-Dmd^{mdx}/J mice were bred and maintained as homozygous animals in standardized conditions in the Animal Resources Core at The Research Institute at Nationwide Children's Hospital. Mice were maintained on Teklad Global Rodent Diet (3.8% fiber, 18.8% protein, 5% fat chow) with a 12-h dark/12-h light cycle. All mice used in this study were male.

Micro-dystrophin gene construction

For all gene transfer studies, the human micro-dystrophin cassette contained the (R4–R23/Δ71–78) domains as previously described.[35] The complementary DNA was codon optimized for human usage and synthesized by GenScript (Piscataway, NJ). It includes a consensus Kozak sequence, an SV40 intron, and synthetic polyadenylation site (53 base pairs). The recombinant MHCK7 promoter used to drive transgene expression is a dual striated muscle-specific promoter and is based on the MCK promoter and the promoter described by Dr. Stephen Hauschka (University of Washington, Seattle, WA).[32] This MCK-based promoter utilizes an enhancer derived from the 5′ of the transcription start site within the endogenous muscle CK gene with a proximal promoter.[32] This enhancer, along with a modified CK7 cassette from the MCK family of genes, is ligated to an α-MHC enhancer 5′ of the CK portion to promote cardiac expression.[32] The MHCK7 micro-dystrophin expression cassette was cloned between AAV2 inverted terminal repeats (ITRs) using

flanking *Xba*I restriction enzyme sites. *Msc*I/*Sma*I restriction enzyme digestions, as well as Sanger sequencing through the ITRs, were used to confirm ITR integrity.

AAV vector production

rAAVrh74.MHCK7.micro-dystrophin was packaged into AAV serotype rh74 capsid using the standard triple transfection protocol as previously described.[31,36,37] A quantitative polymerase chain reaction (qPCR)-based titration method was used to determine an encapsulated vector genome (vg) titer utilizing a Prism 7500 Fast TaqMan detector system (PE Applied Biosystems).[38]

In vivo gene delivery

The mice in this study were randomized in sequential order and dosed per mean body weight per group. *Mdx* mice were injected in the tail vein at 4 to 5 weeks of age with Lactated Ringer (LR) solution (untreated, *mdx*-LR, $n=6$) or with rAAVrh74.MHCK7.micro-dystrophin at escalating doses: 2×10^{12} vg total dose, 8×10^{13} vg/kg ($n=5$); 6×10^{12} vg total dose, 2×10^{14} vg/kg ($n=8$); or 1.2×10^{13} vg total dose, 6×10^{14} vg/kg ($n=8$). Each cohort of mice was necropsied at 12 weeks postvector delivery for histological, functional, and expression analysis. A separate cohort of mice, also injected at 4 to 5 weeks of age with the intermediate dose (6×10^{12} vg) ($n=8$), was necropsied at 24 weeks postvector delivery for long-term analysis of histological, functional, and expression outcome measures. All data acquisition and analysis were blinded to treatment group.

Hematology

Whole blood was obtained from cardiac puncture for serum chemistry panel analysis for C57BL/6 wild-type (WT), *mdx*-LR, intermediate dose (6×10^{12} vg) and high dose (1.2×10^{13} vg). Blood was collected into a serum separating tube and centrifuged for 10 min at 15,000 rpm. Supernatant was collected, frozen, and sent to Charles River Laboratories for chemistry testing. Due to limited sample volume, liver enzymes and glucose chemistries were prioritized.

Histopathology

Following euthanization, necropsy was performed, and organ samples were collected. Muscle tissue was fresh frozen in liquid nitrogen-cooled methylbutane, and all other organs were harvested, fixed in formalin, and embedded in paraffin. After processing, tissues were stained with hematoxylin and eosin, and slides and all tissues were sent to GEMPath, Inc., for blinded histopathology evaluation by a veterinary pathologist. The pathologist was subsequently unblinded for data analysis and report development.

Diaphragm tetanic contraction for functional assessment

Mice were euthanized, and the diaphragm (DIA) was dissected with rib attachments and central tendon intact and placed in Kreb's–Henseleit (K-H) buffer as previously described.[39–43] One 2–4 mm wide section of DIA was isolated per animal per cohort (for one animal in the intermediate dose, two strips were analyzed). DIA strips were tied firmly with braided surgical silk (4-0; Surgical Specialties, Reading, PA) at the central tendon and sutured through a portion of rib bone affixed to the distal end of the strip. Each muscle was transferred to a water bath filled with oxygenated K-H solution that was maintained at 37°C. The muscles were aligned horizontally and tied directly between a fixed pin and a dual-mode force transducer-servomotor (305C; Aurora Scientific, Aurora, Ontario, Canada). Two platinum plate electrodes were positioned in the organ bath, to flank the length of the muscle. The muscle was stretched to an optimal resting tension of 1 g force (the current was set to 1A for duration of the analysis). The muscle was then allowed to rest for 5 min before initiation of the tetanic protocol.

Once the muscle was stabilized, it was subjected to a warm-up, which consisted of three 1-Hz twitches every 30 s, followed by three 150-Hz twitches every minute. After a 3-min rest period, the DIA was stimulated at 20, 50, 80, 120, 150, and 180 Hz, allowing a 2-min rest period between each stimulus, each with a duration of 250 ms to determine maximum tetanic force. Muscle length and weight were measured to determine cross-sectional area. The specific force was normalized to the cross-sectional area of the muscle.

Tibialis anterior tetanic contraction for functional assessment

The tibialis anterior (TA) procedure followed the protocol listed in Hakim *et al.*[44] Mice were anesthetized using a ketamine/xylazine mixture. A double square knot was tied around the patellar tendon with a 4-0 suture. The TA distal tendon was then dissected out, a double square knot was tied around the tendon with 4-0 suture as close to the muscle as possible, and then the tendon was cut. The exposed muscle was constantly dampened with saline. Mice were then transferred to a thermal-controlled platform and maintained at 37°C. The knee was secured by placing a metal pin behind the patellar tendon. The suture attached to the distal TA tendon was pulled to a resting tension of 3 g and adjusted to be level with the arm of the force transducer (Aurora Scientific, Aurora, Canada). An electrode was placed near the sciatic nerve to stimulate it.

Once the muscle was stabilized, the resting tension was set to a force (optimal length) where twitch contractions were maximal. To determine the optimal length resting tension was set at 2, 3, 4, 5, and 6 g force and stimulated at 1 Hz to determine the optimal tension to be used throughout the procedure protocol (the current was set to 200 mA for duration of the analysis). After a 3-min rest period, the TA was stimulated at 50, 100, 150, and 200 Hz, allowing a 1-min rest between each stimulus. Following a

5-min rest, the muscles were then subjected to a series of 10 isometric contractions, occurring at 1-min intervals with a 10% stretch–relengthening procedure. After the eccentric contractions, the mice were euthanized, and the TA muscle was dissected out and frozen for histology.

Immunofluorescence

Cryosections (12 μm) from the TA, gastrocnemius (GAS), quadriceps (QD), psoas major (PSO), gluteus (GLUT), triceps (TRI), and DIA muscles along with the heart were subjected to immunofluorescent staining for the dystrophin transgene through our previously used protocol.[39] Sections were incubated with a mouse monoclonal human dystrophin primary antibody (Santa Cruz Biotechnology, Dallas, TX) at a dilution of 1:50 and the human β-sarcoglycan primary antibody (Leica Biosystems, Buffalo Grove, IL) at a dilution of 1:100. Additional detail about antibodies used for immunofluorescence analysis is shown in Supplementary Table S1. Analysis for percentage of fibers positive for dystrophin staining included 4 random 20X images covering the four different quadrants of the muscle section per animal per tissue ($n=5$ per cohort). Images were taken using a Zeiss AxioCam MRC5 camera (Germany). Percentage of fibers positive for dystrophin staining (>50% of muscle membrane staining) was determined for each image. Quantification data of immunofluorescent-positive fibers expressing dystrophin protein are reported as mean ± standard error of the mean of $n=5$ per treatment group.

Western blot analysis

Western blots were performed according to our previously used protocol, with several modifications specific for each antibody used.[39] Samples from WT mice, *mdx*-LR mice, and vector-dosed *mdx* mice were used for each western blot. Protein (50 μg for muscle and organs) extracted from samples was separated by sodium dodecyl sulfate–polyacrylamide gel electrophoresis (SDS-PAGE) (3–8% Novex NuPAGE gradient gels, Invitrogen, Waltham, MA), blotted on polyvinylidene fluoride membrane, and probed with dystrophin primary antibody Dys1 for dystrophin detection and Dys3 for micro-dystrophin (Leica Biosystems) at a dilution of 1:50 and 1:20, respectively, or neuronal nitric oxide synthase (nNOS) primary antibody (Fisher Scientific) at a dilution of 1:1,000. Loading controls used included γ-tubulin antibody (Sigma) or α-actinin antibody (Sigma) at a dilution of 1:10,000 followed by Alexa Fluor 680 goat anti-mouse (1:5,000, LI-COR, Lincoln, Nebraska). Additional detail about antibodies used for western blot analysis is shown in Supplementary Table S1.

Morphometric analysis

Hematoxylin and eosin staining was performed on 12-μm cryosections of muscle from WT mice, *mdx*-LR mice, and rAAVrh74.MHCK7.micro-dystrophin-treated *mdx* mice for analysis. Muscle fiber diameters were measured using minimal Feret's diameter in all muscles. Analysis for fiber diameters included 4 fields of 20X magnification per animal per side per tissue (low dose, $n=4$; intermediate and high dose, $n=8$; *mdx*-LR and WT, $n=6$). There was a range of 1,000–5,000 fibers quantified per muscle from each treatment group and control cohorts. In addition, the percentage of myofibers with central nuclei was determined analyzing four fields of 20X image magnification per animal from the left side for TA, GAS, QD, PSO, GLUT, TRI, and DIA muscles (low dose, $n=5$; intermediate dose, $n=6$; and high dose, $n=7$; *mdx*-LR and WT, $n=6$). Images were taken with a Zeiss AxioCam MRC5 camera. Fiber diameters were measured using Zeiss AxioVision LE4 software, and centrally nucleated fibers were quantified using the National Institutes of Health ImageJ software.

Biodistribution qPCR analysis

TaqMan qPCR was performed to quantify the number of vg copies present in targeted muscle, as well as nontargeted organs, as previously described.[34,45,46] Biodistribution analysis was performed on tissue samples collected from three vector-dosed *mdx* animals per dose level. Tissues were harvested at necropsy, and vector-specific primer probe sets specific for sequences of the MHCK7 promoter were utilized. A vector-specific primer probe set was used to amplify a sequence of the intronic region directly downstream from the MHCK7 promoter that is unique and located within the rAAVrh74.MHCK7.micro-dystrophin transgene cassette. A positive signal was defined as anything ≥100 single-stranded DNA copies/μg genomic DNA detected. Copy number is reported as vg/μg genomic DNA.

Picrosirius red stain and collagen quantification

Frozen sections placed onto Fisherbrand Superfrost charged microscope slides were fixed in 10% neutral buffered formalin for 5 min and then rinsed in distilled water. Slides were then incubated in Solution B (Direct Red 80/2 4 6-Trinitrophenol) from the Picrosirius Red Stain Kit (Polysciences, Inc., Mount Arlington, NJ, Catalog no. 24901) for 15 min. After a thorough rinse in distilled water, the slides were placed in Solution C (0.1 N hydrochloride acid) for 2 min. Slides were counterstained for 5 min with 1% Fast Green in 1% glacial acetic acid from Poly Scientific (Bay Shore, NY, Catalog no. S2114) using a 1:10 dilution in deionized water. Finally, the slides were rinsed again in distilled water, dehydrated in graded ethanol, cleared in xylene, and mounted with coverslips using Cytoseal 60 media from Thermo Scientific (Catalog no. 8310). Images were taken using the AxioVision 4.9.1 software. Representative images of DIA tissue sections in *mdx* mice treated with rAAVrh74.MHCK7.micro-dystrophin were compared to *mdx*-LR mice at 20X magnification.

For analysis of Sirius red staining and percent collagen quantification, the contrast between the red and the green colors was enhanced using Adobe Photoshop. The color deconvolution plugin in the ImageJ software program was selected, and the RGB color deconvolution option was used. The red image includes all connective tissue from the Sirius red stain. The green image includes all muscle from the Fast Green counterstain. Only the red image and the original image were used. A threshold was applied to the images to obtain black and white images with areas positive for collagen in black and negative areas in white. Using the measure function, the area of collagen was calculated. The total tissue area was determined by converting the original image to ''8-bit'' and adjusting the threshold to 254 (one unit below completely saturating the image). The total tissue area was measured as done previously, and total area was recorded. Quantification of collagen accumulation in the DIA of WT mice, *mdx*-LR, and mice treated with low (2×10^{12} vg), intermediate (6×10^{12} vg), and high (1.2×10^{13} vg) doses was calculated by dividing the area of collagen by total tissue area and used to determine the mean percentage for each individual ($n=5$, low dose; $n=8$, intermediate and high dose; $n=6$, *mdx*-LR; and $n=5$, WT).

Statistical analysis

Data are expressed as the mean ± standard error of the mean (SEM; error bars) and were analyzed using a one-way analysis of variance (ANOVA) or two-way ANOVA with multiple comparisons between groups and statistical significance determined through Tukey's *post hoc* analysis test using GraphPad Prism 5 (GraphPad Software, La Jolla, CA), unless otherwise specified.

RESULTS

Our micro-dystrophin transgene cassette was constructed by replacing the MCK promoter from previous studies with the MHCK7 promoter to enhance cardiac expression.[34] To establish the minimal efficacious dose *in vivo*, a dose-escalation study was performed. The dosing groups included a low dose of 2×10^{12} vg total, intermediate dose of 6×10^{12} vg total, and high dose of 1.2×10^{13} vg total. These doses were kept consistent throughout the study, and efficacy was determined through systemic delivery to the tail vein of *mdx* mice.

Histological improvements with systemic delivery in a dose-dependent manner

Four- to five-week-old *mdx* mice were treated with low, intermediate, or high total dose of rAAVrh74.MHCK7.micro-dystrophin intravenously in the tail vein. Mice were necropsied 3 months postinjection, and micro-dystrophin transgene expression was demonstrated using immunofluorescent staining in both the left and right side skeletal muscles, including TA, GAS, QD, PSO, TRI, and GLUT. In addition, the DIA and heart were analyzed. Immunofluorescent staining showed robust micro-dystrophin expression at the sarcolemma membrane of skeletal and cardiac muscle after systemic delivery of rAAVrh74.MHCK7.microdystrophin; representative immunohistochemistry images are shown at the intermediate dose (6×10^{12} vg total) in Fig. 1A and Supplementary Fig. S1. Micro-dystrophin expression levels in each individual muscle type were averaged from all treated mice. The mean percentage expression of micro-dystrophin positive fibers in treated mice was $46.7\%\pm8.08\%$, $66.8\%\pm6.18\%$, and $78.3\%\pm4.7\%$ for low, intermediate, and high dose, respectively, across all muscles (data represented as mean ± SEM, Fig. 1B). For all doses we observed high-level expression in the heart, with intermediate and high dose resembling WT expression levels in all animals (Fig. 1A and Supplementary Fig. S1). Importantly, the variation of micro-dystrophin positive fiber expression across each animal per cohort ($n=5$) in each tissue was not statistically different within dosing cohorts (less than 10% difference). We also assessed the restoration of additional DAPC components in skeletal muscle (*e.g.*, TA) following micro-dystrophin gene transfer and found restoration of β-sarcoglycan in addition to dystrophin expression (Fig. 1A).

Fibrosis and inflammation have been previously reported in *mdx* muscle as part of the chronic dystrophic process. Therefore, fiber diameter, fibrosis, and central nucleation (CN) were evaluated postinjection to evaluate the muscle environment postvector delivery compared to *mdx*-LR mice. Gene transfer significantly reduced pathological severity at intermediate and high vector doses administered. Furthermore, gene transfer showed reduction of dystrophic features, including fibrosis (Fig. 2A and Supplementary Fig. S2A), and normalization of fiber size distribution with a significant increase in fiber diameter, indicating fiber size similar to WT fibers, specifically in the DIA, where results for low and intermediate doses were not significantly different from the WT. We also observed a normalization of fiber size in the TA for low and high doses and at the intermediate dose for the TRI (Fig. 2B and Supplementary Fig. S2B). Quantification of histological parameters demonstrated a significant reduction in CN in all skeletal muscles analyzed in a dose-dependent manner compared to *mdx*-LR mice. Gene transfer did not result in complete normalization to WT, and CN remains significantly higher in treated animals but we observed a significant improvement in the TA and GAS of the high dose cohort (Supplementary Fig. S2C).

In addition, Sirius red quantification, which represents the amount of collagen deposition in skeletal muscle, was measured to assess the effect of gene transfer on fibrosis (Fig. 3A). Gene transfer with rAAVrh74.MHCK7.micro-dystrophin decreased collagen deposition in the DIA, showing an

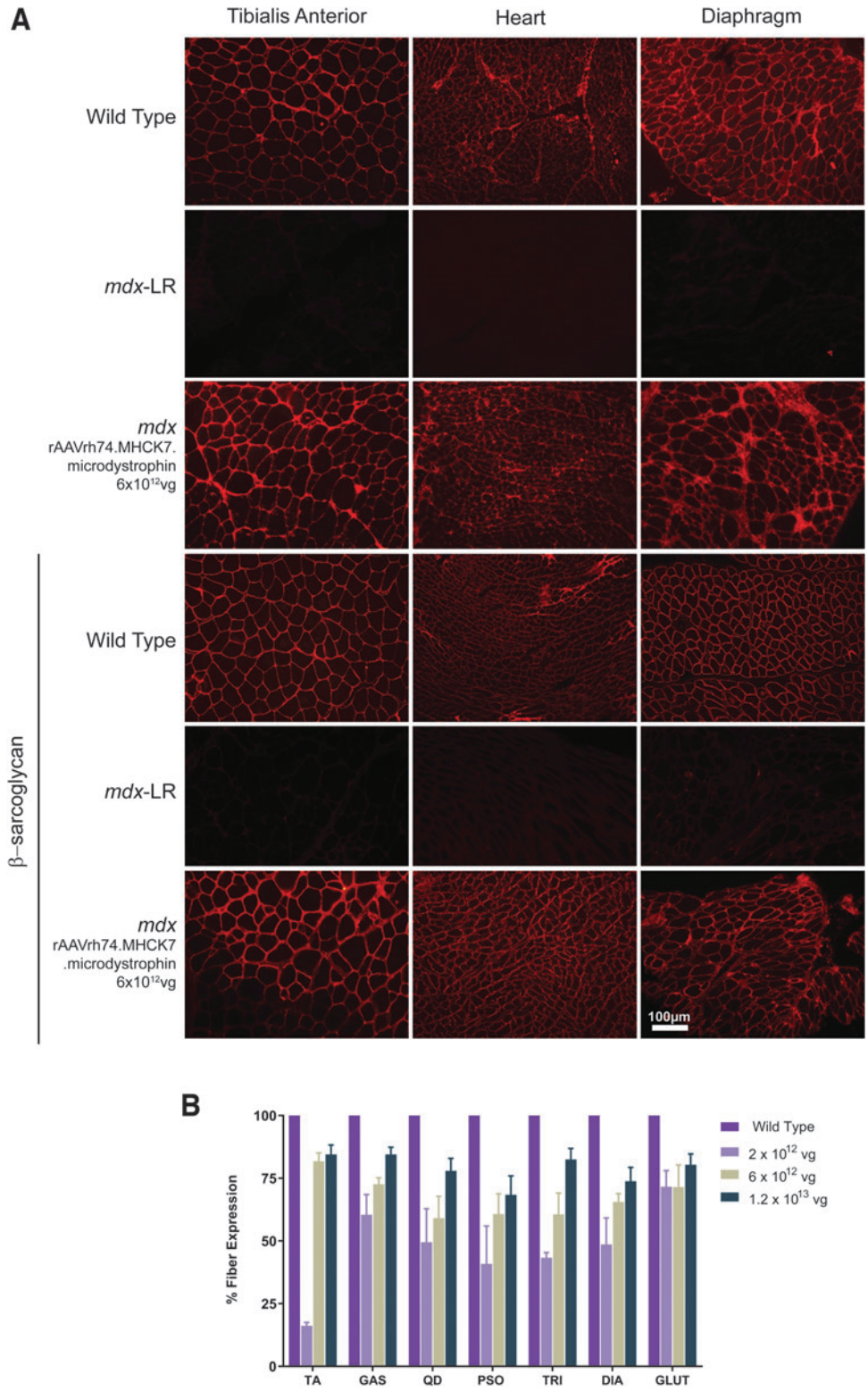

Figure 1. Robust micro-dystrophin expression at the sarcolemma membrane of skeletal and cardiac muscle after systemic delivery of rAAVrh74.MHCK7.micro-dystrophin. Mice received rAAVrh74.MHCK7.micro-dystrophin intravenously at 2.0×10^{12} vector genome (vg) total (low), 6×10^{12} vg total (intermediate), and 1.2×10^{13} vg total (high) dose. **(A)** Representative immunohistochemistry images are shown at the intermediate dose of 6×10^{12} vg total. Immunofluorescent staining for micro-dystrophin using an N-terminal dystrophin antibody in the TA, heart, and DIA 3 months postinjection compared to Lactated Ringer's (vehicle)-treated *mdx* mice (second *row* panel). β-sarcoglycan staining in the treated cohorts represent rescue of the dystrophin-associated protein complex. **(B)** Quantification of immunofluorescent-positive fibers expressing dystrophin protein. Data are reported as mean $\pm$ SEM of $n=5$ per treatment group. DIA, diaphragm; GAS, gastrocnemius; GLUT, gluteus; *mdx*-LR, Lactated Ringer's (vehicle)-treated *mdx*; PSO, psoas major; QD, quadriceps; SEM, standard error of the mean; TA, tibialis anterior; TRI, triceps.

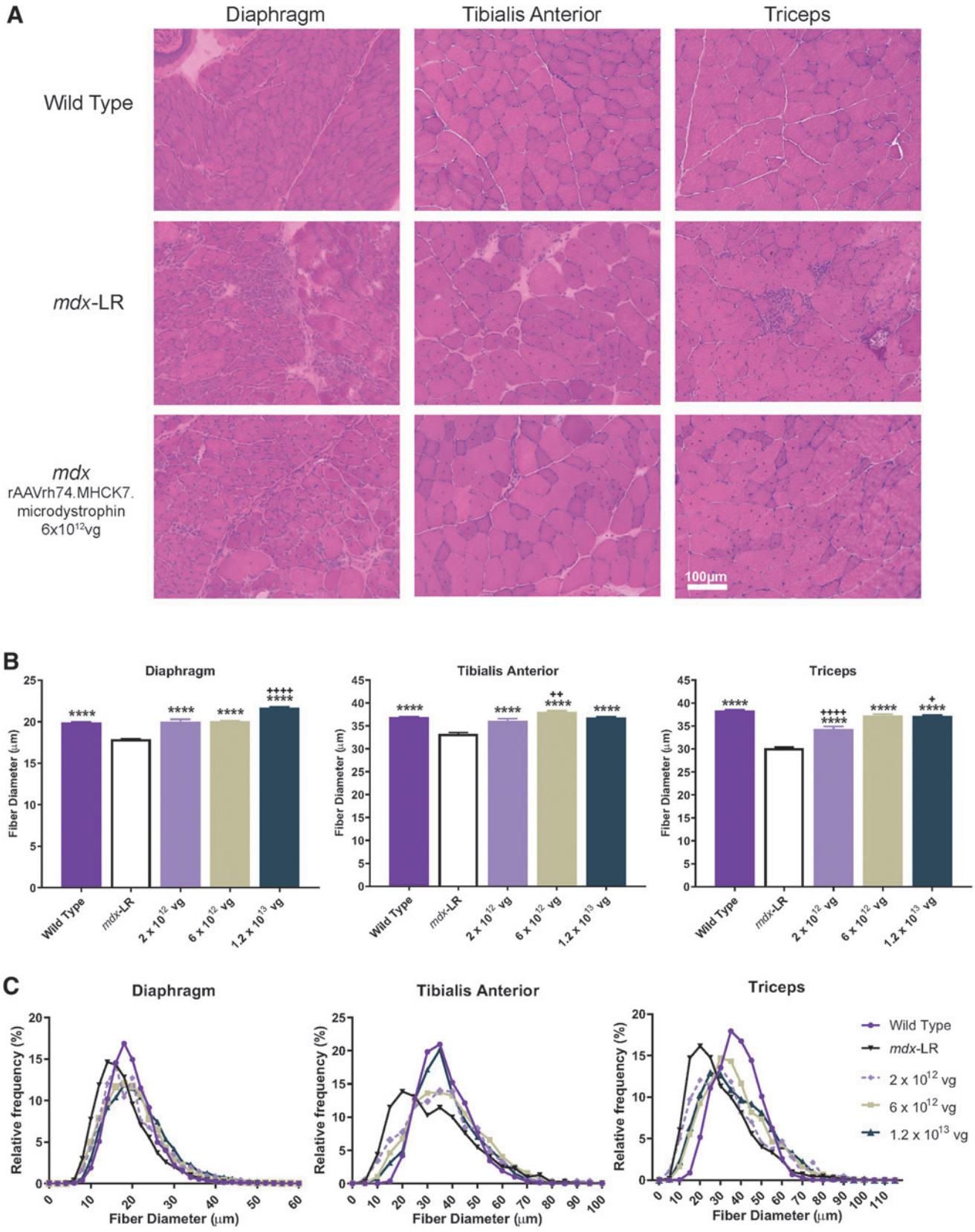

Figure 2. Systemic treatment with rAAVrh74.MHCK7.micro-dystrophin improves muscle pathology in *mdx* mice. Hematoxylin and eosin staining to detect morphology. **(A)** Representative images of diaphragm, tibialis anterior, and triceps muscle from WT mice, Lactated Ringer's (vehicle)-treated *mdx* mice (*mdx*-LR mice), and rAAVrh74.MHCK7.micro-dystrophin-treated *mdx* mice at the intermediate dose of 6×10^{12} vg total. **(B, C)** Quantification of average fiber size and frequency distribution demonstrates a normalization of fiber size across all of the assessed tissues (*i.e.*, diaphragm, tibialis anterior, and triceps) in the *mdx* mice treated with rAAVrh74.MHCK7.micro-dystrophin at total dose of 2×10^{12} vg, 6×10^{12} vg, and 1.2×10^{13} vg. Data reported in bar graph as mean ± SEM ($n=4$ low dose ($SD_{DIA}=7.4$, $SD_{TA}=15.1$, $SD_{TRI}=17.3$); $n=8$ intermediate dose ($SD_{DIA}=7.2$, $SD_{TA}=14.1$, $SD_{TRI}=15.2$) and high dose ($SD_{DIA}=7.9$, $SD_{TA}=12$, $SD_{TRI}=15.8$); $n=6$ *mdx*-LR ($SD_{DIA}=6.6$, $SD_{TA}=15.8$, $SD_{TRI}=15.1$); and WT ($SD_{DIA}=5.6$, $SD_{TA}=10$, $SD_{TRI}=10.6$)). Data were analyzed by one-way ANOVA followed by Tukey's *post hoc* analysis. ****$=p<0.0001$ versus *mdx*-LR mice. +$=p<0.5$; ++$=p<0.005$; ++++$=p<0.0001$ versus WT. ANOVA, analysis of variance; SD, standard deviation; WT, wild-type.

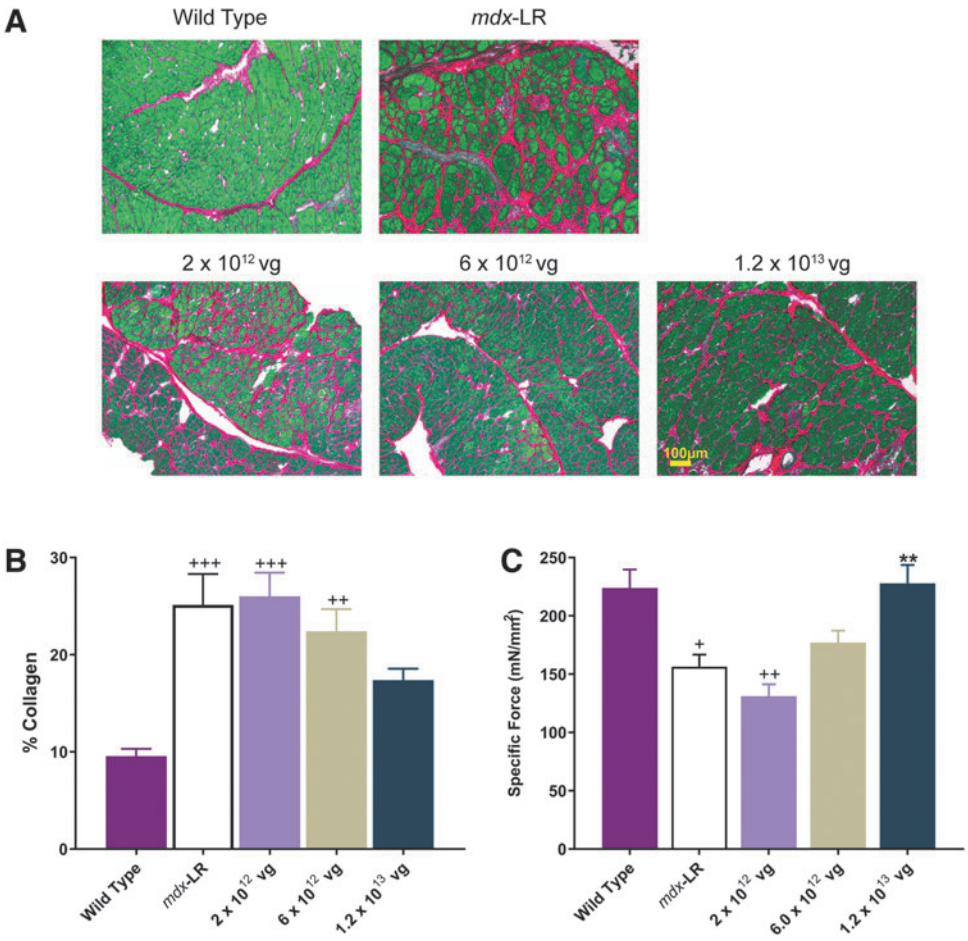

Figure 3. Reduction of fibrosis after systemic treatment with rAAVrh74.MHCK7.micro-dystrophin is associated with improvement in DIA muscle function. Muscle tissue sections were stained using picrosirius red stain to assess collagen content. **(A)** Representative images of DIA tissue sections in WT mice, Lactated Ringer's (vehicle)-treated *mdx* mice (*mdx*-LR mice), and *mdx* mice treated with rAAVrh74.MHCK7.micro-dystrophin with low (2×10^{12} vg), intermediate (6×10^{12} vg), and high (1.2×10^{13} vg) doses. **(B)** Quantification of collagen accumulation (%) in the DIA of WT mice, *mdx*-LR mice, and *mdx* mice treated with rAAVrh74.MHCK7.micro-dystrophin ($n=5$, low dose; $n=8$, intermediate and high dose; $n=6$, *mdx*-LR; and $n=5$, WT). **(C)** DIA muscle function in WT mice, *mdx*-LR mice, and *mdx* mice treated with rAAVrh74.MHCK7.micro-dystrophin ($n=5$, low dose; $n=9$, intermediate; $n=8$, high dose; $n=8$, *mdx*-LR; and $n=5$, WT). Following 3 months of treatment, DIA muscle strips were harvested to measure specific force (normalized to cross-sectional area). For panels **B** and **C**, data are represented as mean ± SEM and were analyzed by one-way ANOVA followed by Tukey's *post hoc* analysis. ** = $p<0.005$ versus *mdx*-LR mice; + = $p<0.05$, ++ = $p<0.005$, +++ = $p<0.001$ versus WT mice.

increasing improvement compared to the untreated mice with no significant differences between the highest dose and the WT (Fig. 3B), which corresponded to a significant increase in force output of the DIA to levels comparable to that observed in WT mice (Fig. 3C). Finally, to evaluate the presence of any additional histopathology in the skeletal muscles due to vector delivery, an alpha sarcomeric actin immunofluorescent stain was used to evaluate any incidence of ringed fibers. Previously, others have described incidences of ringed fibers in the neuromuscular junction or the GAS with the inclusion of a micro-dystrophin construct that contains the H2 region.[35,47,48] After a thorough analysis of all skeletal muscles, there were no instances of ringed fibers or abnormal histopathology in *mdx* mice after treatment with rAAVrh74.MHCK7.micro-dystrophin (Supplementary Fig. S3).

Functional improvements with systemic delivery in dose-dependent manner

To determine whether micro-dystrophin gene transfer provides a functional benefit to diseased muscle, we assessed the properties of both the DIA (Fig. 3C) and TA (Fig. 4A, B) muscles from WT mice, *mdx*-LR mice, and rAAVrh74.MHCK7.micro-dystrophin-treated mice at the three dose levels. Tail vein delivery of rAAVrh74.MHCK7.micro-dystrophin led to a stepwise improvement in specific force output in the DIA (176.9 mN/mm^2 in the intermediate-dose group vs. 227.78 mN/mm^2 in the high-dose group) that was comparable to WT levels for the higher dose. Furthermore, it was demonstrated that, for the TA muscle, there were functional deficits in *mdx*-LR mice compared with WT mice with a 58% decrease in force output (171.3 vs. 291.65 mN/mm^2)

and greater loss of force following eccentric contractions (32% loss in *mdx*-LR mice; 5% loss in WT mice). Administration of rAAVrh74.MHCK7.micro-dystrophin resulted in a significant improvement in force output and rescue from contraction-induced damage in the TA muscles after rigorous eccentric contraction exercise. Finally, the systemic delivery of the rAAVrh74.MHCK7.micro-dystrophin construct, which contains the critical force producing spectrin repeats R1–R3, demonstrates increased force generation in the TA and DIA. Furthermore, micro-dystrophin significantly protected muscle membranes from damage, as evidenced by a 75% reduction of creatine kinase (CK) (Fig. 4C).

In addition to sarcoglycan proteins, we also evaluated other DAPC-associated components, such as nNOS, using western blot analysis. Although the micro-dystrophin construct does not contain spectrin repeats 16 and 17, which have been identified as one of the sarcolemmal nNOS-specific sites,[49,50] when analyzing nNOS protein expression by western blot for all muscles analyzed in treated animals ($n=2$ analyzed), we found the amount of nNOS protein in skeletal muscle to be equal to the amount found in WT TA tissues and increased compared to the untreated *mdx* mouse (Fig. 5A).

Vector biodistribution following systemic delivery

To confirm the presence of test article-specific DNA sequences, biodistribution analysis was examined using real-time qPCR. Figure 5B depicts the vg copies detected in each tissue sample from rAAVrh74.MHCK7.micro-dystrophin-injected mice. rAAVrh74.MHCK7.micro-dystrophin transcript was detected at varying levels in all collected tissues. As expected, the highest levels were seen in skeletal muscle and the heart, as well as clearance organs. The lowest levels were detected in gonad, lung, and kidney in all dose levels. Western blot was used to detect the transgene micro-dystrophin protein in tissue samples. Micro-dystrophin protein was observed across all skeletal muscles analyzed, with the highest amount in the heart for intermediate and high dose (representative Fig. 5C, full blot in Supplementary Fig. S5, additional animal blots in Supplementary Fig. S6). Importantly there was no micro-dystrophin protein detected in the intermediate and high dose cohorts in any off-target organs. We observed a faint band in the liver at the highest dose, which could be at the lower limit of detection. Finally, there were no adverse histopathologic effects noted in the liver by the independent pathologist and no abnormal blood chemistries in any of the dosed cohorts (Supplementary Fig. S4).

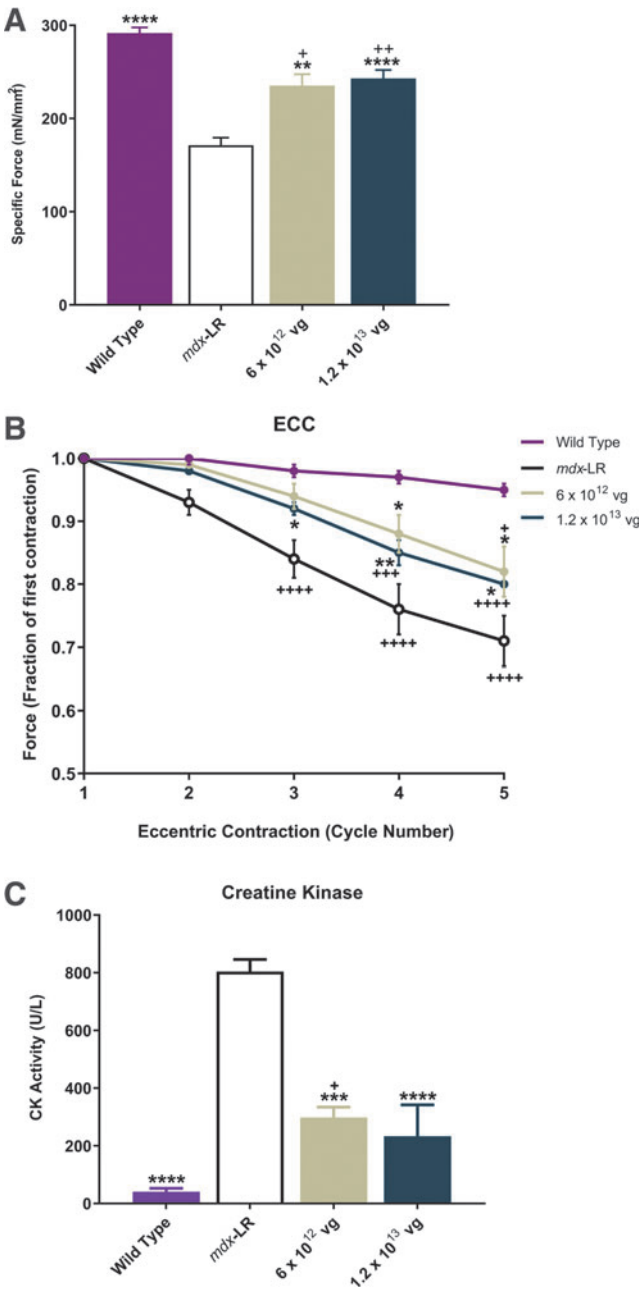

Figure 4. Functional benefits to skeletal muscle in intermediate- and high-dose cohorts. **(A)** Specific muscle force in TA muscles (normalized to cross-sectional area) assessed 3 months after treatment with rAAVrh74.MHCK7.micro-dystrophin (*left* and *right* side per animal, per cohort: $n=8$, intermediate dose (6×10^{12} vg); $n=16$, high dose (1.2×10^{13} vg); $n=14$, Lactated Ringer's (vehicle)-treated *mdx* (*mdx*-LR); $n=9$, WT). **(B)** Eccentric force loss in TA muscle assessed using a rigorous ECC protocol. Force output is plotted at each cycle (mean of *left* and *right* side per animal, per cohort: $n=8$, intermediate dose; $n=13$, high dose; $n=13$, *mdx*-LR; $n=9$, WT). **(C)** Serum CK levels 3 months post-treatment ($n=2$, intermediate and high dose; $n=5$, *mdx*-LR and WT). For panels **A** and **C**, data are represented as mean ± SEM and analyzed by one-way ANOVA followed by Tukey's *post hoc* analysis for multiple comparisons. $**=p<0.01$, $***=p<0.001$, and $****=p<0.0001$ versus *mdx*-LR mice; $+=p<0.05$, $++=p<0.005$, $+++=p<0.001$, $++++=p=0.0001$ versus WT mice. In panel **B**, data are represented as mean ± SEM and analyzed by two-way ANOVA followed by Tukey's *post hoc* analysis for multiple comparisons. $*=p<0.05$, $**=p<0.01$ versus *mdx*-LR mice; $+=p<0.05$, $+++=p<0.001$, $++++=p=0.0001$ versus WT mice. CK, creatine kinase; ECC, eccentric contraction cycle.

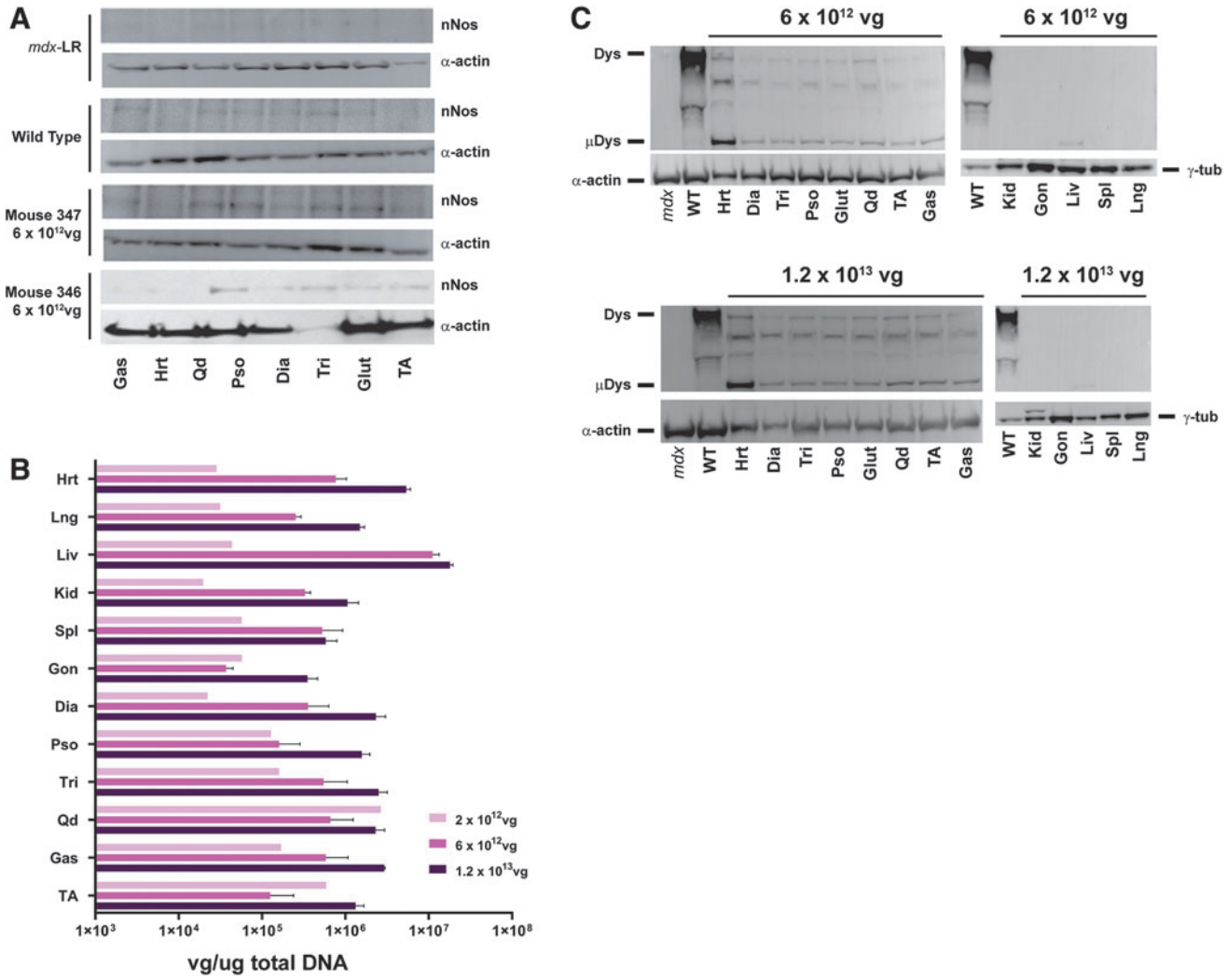

Figure 5. Biodistribution of vgs and protein expression in vector-treated mice. **(A)** Representative western blot of nNOS protein expression in muscle tissues of Lactated Ringer's (vehicle)-treated *mdx* mice, WT mice, and two mice (Mouse 347 and Mouse 346) treated with 6×10^{12} vg total dose of rAAVrh74.MHCK7.micro-dystrophin (intermediate). **(B)** Biodistribution of vgs normalized to microgram of DNA in organs and tissues after systemic delivery of rAAVrh74.MHCK7.micro-dystrophin ($n=3$ for each cohort). Data are represented as mean ± SEM. **(C)** Western blot analysis of dystrophin protein expression in muscles and organs from mice 3 months after treatment with rAAVrh74.MHCK7.micro-dystrophin at an intermediate (6×10^{12} vg) and high (1.2×10^{13} vg) dose. α-actinin and γ-tubulin were used as loading controls. α-actin, α-actinin; Dys, dystrophin; γ-tub, γ-tubulin; Glut, gluteus; Gon, gonads; Hrt, heart; Kid, kidney; Liv, liver; Lng, lung; μDys, micro-dystrophin; *mdx*-LR, Lactated Ringer's (vehicle)-treated *mdx*; nNOS, neuronal nitric oxide synthase; Spl, spleen.

Durable improvements following a single systemic infusion

A cohort of *mdx* male mice were injected with an intermediate dose (6×10^{12} vg) at 4 weeks of age and necropsied at 6 months postinjection to evaluate long-term expression and functional benefit of a single intravenous treatment with rAAVrh74.MHCK7.micro-dystrophin. Micro-dystrophin transgene expression was demonstrated using immunofluorescent staining for micro-dystrophin using an N-terminal dystrophin antibody in skeletal muscle (TA), heart, and DIA (Fig. 6A). Histology was analyzed by hematoxylin and eosin staining (Fig. 6B). Micro-dystrophin transgene expression was also evaluated by immunofluorescence in six skeletal muscles (TA, GAS, QD, PSO, TRI, GLUT), both left and right, in addition to the DIA of all treated mice. Systemic delivery of an intermediate dose (6×10^{12} vg) of rAAVrh74.MHCK7.micro-dystrophin resulted in 65.5% fibers localized to the membrane with micro-dystrophin in the TA muscle (Fig. 6C) and an increase of specific force output, which improved to 235.4 mN/mm^2 and protected the muscle from repeated eccentric contraction damage with only a 25% decrease in force (Fig. 6D). These results demonstrate that there was preservation of transgene expression 6 months postinjection, as well as no decrease in functional benefits observed at earlier time points in both the DIA and TA, suggesting sustained effects (long-term durability) after a single administration.

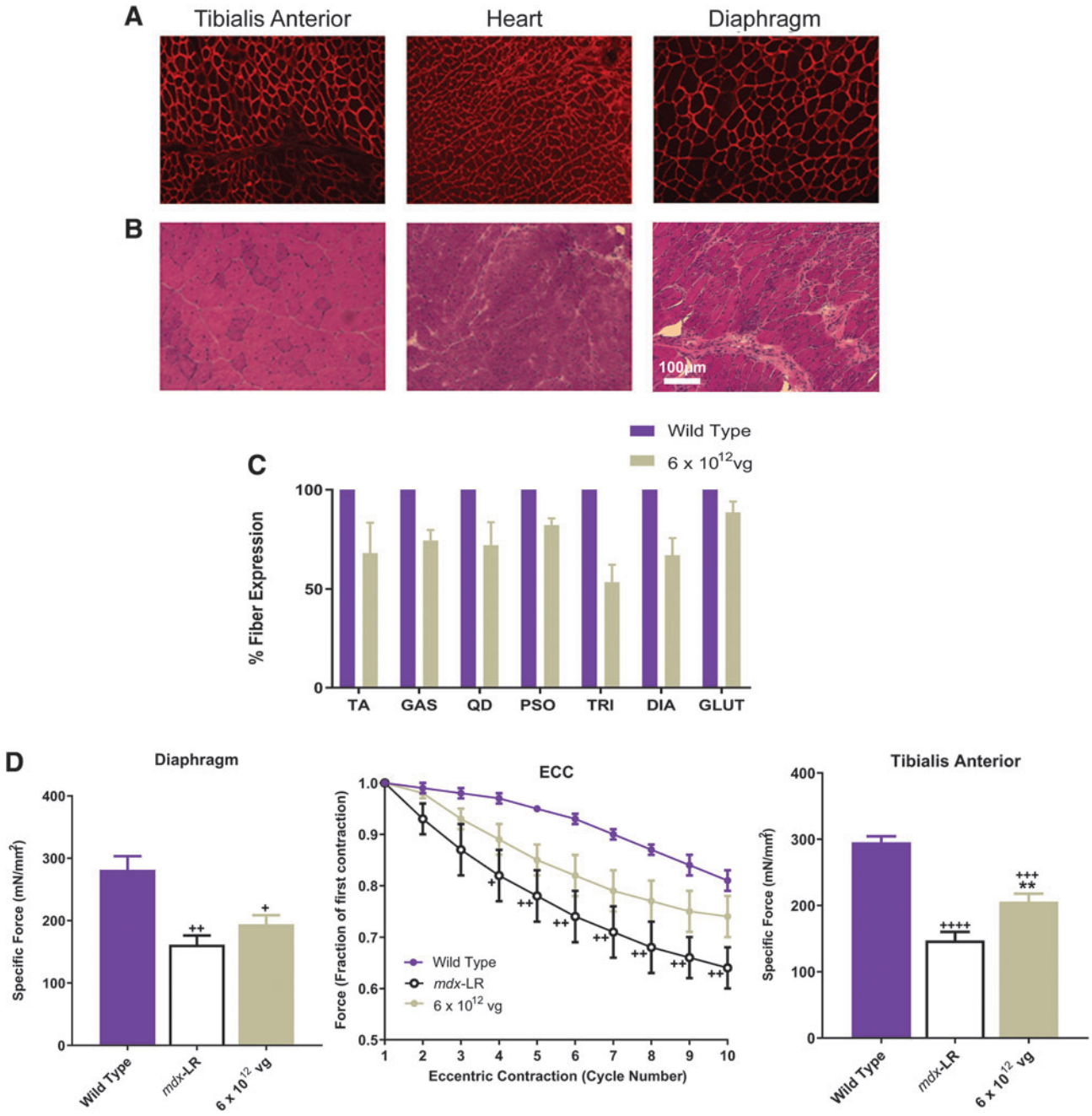

Figure 6. Long-term durability after a single administration of rAAVrh74.MHCK7.micro-dystrophin in *mdx* mice. **(A, B)** Representative immunofluorescent staining for micro-dystrophin using an N-terminal dystrophin antibody and hematoxylin and eosin stained TA, heart, and DIA of *mdx* mice treated with rAAVrh74.micro-dystrophin at an intermediate (6×10^{12} vg) dose, 6 months post-treatment. **(C)** Quantification of immunofluorescent-positive fibers expressing micro-dystrophin protein 6 months after a single treatment with rAAVrh74.MHCK7.micro-dystrophin. Data are reported as mean ± SEM of $n=5$. **(D)** Specific force generation in the DIA and TA muscles 6 months after a single treatment with rAAVrh74.MHCK7.micro-dystrophin. Data reported as mean ± SEM of $n=5$. Data were analyzed by one-way ANOVA followed by Tukey's *post hoc* analysis for multiple comparisons. **$=p<0.05$ versus *mdx*-LR mice; +$=p<0.05$, ++$=p<0.005$, +++$=p<0.0005$, ++++$=p<0.0001$ versus WT mice. Eccentric force loss following a rigorous ECC protocol ($n=8$ in each group). Data reported as mean ± SEM. Data were analyzed by two-way ANOVA followed by Tukey's *post hoc* analysis for multiple comparisons. +$=p<0.2$, ++$=p<0.007$ versus WT mice. Glut, gluteus; *mdx*-LR, Lactated Ringer's (vehicle)-treated *mdx*.

DISCUSSION

We have designed a therapeutic human micro-dystrophin cassette packaged into an rAAVrh74 vector, which includes the use of a dual striated muscle-specific promoter to selectively express transgene in skeletal and cardiac muscle. rAAVrh74 is a serotype recently isolated from lymph nodes of rhesus monkeys. rAAVrh74 displays high affinity for skeletal and cardiac muscle tissue,[51,52] and we have previously demonstrated robust biopotency using rAAVrh74 in biodistribution, delivery, and trans-

duction of dysferlin, GALGT, and sarcoglycan proteins for other muscular dystrophies.[36,51–54] In addition, rAAVrh74 seroprevalence is relatively low among other AAV serotypes,[55] which thus allows for application for more patients. Currently, the rAAVrh74 capsid is the vector that we have used in our gene therapy clinical trials in patients with DMD and with limb-girdle muscular dystrophy types 2E/R4, 2D/R3, and 2B/R2 (NCT02376816, NCT03769116, NCT03652259, NCT01976091, NCT02710500).

The safety and efficacy of AAV gene therapy for neuromuscular diseases are not only dictated by vector delivery (*e.g.*, biodistribution and tissue uptake) but also by regulation of transgene expression in the targeted tissue (*i.e.*, skeletal and cardiac muscle). Use of selective promoters is essential to maximize gene expression in targeted tissues and limit expression in nonrelevant tissues. In this study, we used MHCK7, which includes an α-MHC enhancer that has been shown to lead to high levels of expression in cardiomyocytes and increased dystrophin expression in skeletal muscle compared to muscle-specific promoters, MCK or CK7.[32] Indeed, we provide further support that MHCK7 limits off-target transgene expression, as demonstrated by widespread tissue and organ biodistribution of vector genomes, accompanied by micro-dystrophin protein expression limited to skeletal and cardiac muscle. Our findings presented here are consistent with our previous studies that demonstrated robust skeletal and cardiac muscle expression of *β*-sarcoglycan in mice after systemic delivery of the transgene using the rAAVrh74 capsid with expression driven by MHCK7.[39]

In the present study we provide further evidence that demonstrates the translational relevance of systemic delivery of rAAVrh74.MHCK7.micro-dystrophin. Systemic delivery of rAAVrh74.MHCK7.micro-dystrophin demonstrated prevention of dystrophic features at both the intermediate and high doses with reductions in inflammation, fewer degenerating fibers, and improvement in force generation of the DIA and the TA. The reductions in dystrophic histopathology were more marked in the intermediate- and high-dose cohorts, with no significant difference in decreased degeneration and decreased inflammation between the two dosing groups. The DIA revealed the most marked changes in dosed cohorts. The heart exhibited a few small foci of minimal mononuclear cell accumulation in the ventricular myocardium in several dosed animals. However, vector-dosed cohorts had substantially reduced myopathy in all tissues and the heart. Of interest, serum CK levels were significantly reduced after treatment with rAAVrh74.MHCK7.micro-dystrophin, which coincides with the protection we observed from damage due to eccentric contractions in vector-dosed *mdx* mice compared to *mdx*-LR mice.

It must be noted that given the limited DNA packaging capacity of AAV, numerous efforts to develop and evaluate shortened variations of dystrophin have been examined in preclinical animal models. While many constructs have shown success in delivery, varying degrees of expression and functional efficacy have been reported (for review, see Duan[56]). We chose to use a transgene sequence designed to result in production of a protein with optimized functionality. Indeed, the transgene utilized here (ΔR4-23/ΔCT) has been shown to prevent and reverse dystrophic pathology associated in *mdx* mice and protect against damage due to eccentric contractions when delivered using AAV2, AAV6, or AAV8 with expression driven by the cytomegalovirus (CMV) or the muscle-specific promoter, MCK.[34,57,58] This variant of micro-dystrophin includes the N-terminus; spectrin-like repeats R1-3 and R24; hinges 1, 2, and 4; and the cysteine-rich domain. We believe that the ability of R1-3 to interact with the lipid membrane[29,30] may play an important role in maintaining structural integrity and protection of muscle tissue from damage.

In addition, inclusion of hinges is important for conferring flexibility by providing the structural mechanism for dystrophin to function as a shock absorber.[24] Prior studies reported that the presence of hinge 3 in ΔR4-23/ΔCT rescued muscle deterioration and structural deficits at neuromuscular junctions in *mdx* mice.[58] However, there were no differences in restoration of muscle functional capacity between hinge 2 and hinge 3 when configured in micro-dystrophin constructs ΔR4-23/ΔCT and ΔH2-23/ΔCT+H3 in *mdx* mice.[58] Banks *et al.* reported the formation of ringed fibers in *mdx* mice expressing ΔR4-23/ΔCT packaged into AAV6 with expression of the transgene driven by the constitutive CMV promoter.[58] In the present study, we did not observe any instance of ringed fibers in any vector-dosed tissues in mice. The reason for this discrepancy is unclear but could be due to differences in the constructs or technical differences between studies (*e.g.*, age of mice, route of administration). Use of hinge 2 has the advantage of maintaining the natural linkage to the R1–3 domain, whereas use of hinge 3 would create a novel junction. Novel juxtapositions of protein domains may promote immune responses[59] or result in protein misfolding, which in turn may either promote degradation[60,61] or result in formation of protein inclusions.[34,62]

It has been reported that nNOS binding domain R16–17 of dystrophin is essential to restore sarcolemmal nNOS expression in *mdx* mice and canine DMD models, as demonstrated by enhanced muscle perfusion, prevention of functional ischemia, and improvement in muscle force and exercise capacity.[19,28,48,63–65] In contrast, several lines of evidence have also demonstrated that while lack of nNOS expression may be sufficient to promote deterioration, its presence is not required for muscle function or protection from overt dystrophy. For example, mice with genetic loss of nNOSμ did not exhibit skeletal muscle fatigue or loss of specific muscle force,[66] and forced expression of nNOSμ only partially rescued eccentric force loss in mouse models of DMD compared to WT animals.[67] Likewise, the presence of the R16–17 domains in micro-dystrophin

constructs only partially protected the eccentric force loss observed in *mdx* mice.[28] Furthermore, transgenic mouse models that harbor genetic loss of nNOS expression do not overtly display a dystrophic phenotype.[68,69]

In the present study, we analyzed nNOS expression for two treated mice from the intermediate-dose cohort, and the results show increased quantities of nNOS protein in all skeletal muscles compared with *mdx*-LR mice. These results are preliminary and further studies are needed, but suggest that nNOS protein presence in the muscle rather than increased nNOS sarcolemma-specific localization is beneficial for function, as has been previously suggested.[16,17]

Altogether these studies, in conjunction with the present findings, demonstrate the importance in design and configuration of micro-dystrophin.

In addition to efficacy, this dose-escalation study demonstrated minimal toxicity when mice were treated with rAAVrh74.MHCK7.micro-dystrophin at even the highest total dose of 1.2×10^{13} vg. In *mdx*-LR mice there was widespread variable myopathy affecting all seven skeletal muscles, as well as the right ventricular wall of the heart. The principal findings included pronounced and widespread myofiber atrophy (30–75% of normal myofiber size), minimal-to-mild mononuclear cell inflammations, increased interstitial space, and increased cytoplasmic mineral deposits, as concluded by an independent veterinary pathologist. Notably, the lack of abnormal values in evaluation using a serum chemistry panel further provides support for the safety and tolerability to treatment with rAAVrh74.MHCK7.micro-dystrophin.

In conclusion, the findings presented here provide proof of principle for safety and efficacy to support systemic delivery of rAAVrh74.MHCK7.micro-dystrophin at high vector titers and support initiation of a Phase I/II safety study in patients with DMD.

ACKNOWLEDGMENTS

The authors thank the Nationwide Children's Viral Vector Core for Vector Production and Dr. Stephen Hauschka for his gift of the MHCK7 promoter. The authors also thank Terri Shaffer, MLAS, RLATG, for performing intravenous tail vein injections. Medical writing and editorial support were provided by Khampaseuth Thapa, PhD, and Lucia Quintana-Gallardo, PhD, of Sarepta Therapeutics, Inc., and Purvi Kobawala Smith, MS, MPH, of Health & Wellness Partners, LLC, Upper Saddle River, NJ, funded by Sarepta Therapeutics, Inc.

AUTHORS' CONTRIBUTIONS

Conceptualization, R.A.P., J.R.M., and L.R.R.-K.; Methodology, R.A.P., D.A.G., and L.R.R.-K.; Formal analysis, R.A.P; Investigation, R.A.P, D.A.G., K.N.H, E.L.P., and E.K.C.; Resources, R.A.P, D.A.G, L.R.R.-K.; Writing—original draft, R.A.P., and L.R.R.-K.; Writing—review & editing, R.A.P., D.A.G, K.N.H, J.R.M., and L.R.R.-K.; Visualization, R.A.P, D.A.G., J.R.M, and L.R.R.-K.; Supervision, L.R.R.-K.; Project administration, D.A.G.; Funding acquisition, J.R.M. and L.R.R.-K.

AUTHOR DISCLOSURE

R.A.P. is an employee of Sarepta Therapeutics, Inc., D.A.G. is an employee of Sarepta Therapeutics, Inc., K.N.H. and E.K.C.: No competing financial interest exists. E.L.P. is an employee of Sarepta Therapeutics, Inc., J.R.M. is the coinventor of the rAAVrh74.micro-dystrophin technology. This technology has been exclusively licensed to Sarepta Therapeutics, Inc., L.R.R.-K. is the coinventor of the AAVrh74.micro-dystrophin technology and eligible to receive financial consideration as a result. L.R.R.-K. is an employee of Sarepta Therapeutics, Inc.

FUNDING INFORMATION

This study was funded by the Nationwide Children's Hospital Research Foundation, Parent Project Muscular Dystrophy, and Sarepta Therapeutics, Inc.

SUPPLEMENTARY MATERIAL

Supplementary Figure S1
Supplementary Figure S2
Supplementary Figure S3
Supplementary Figure S4
Supplementary Figure S5
Supplementary Figure S6
Supplementary Table S1

REFERENCES

1. Aartsma-Rus A, Straub V, Hemmings R, et al. Development of exon skipping therapies for Duchenne muscular dystrophy: a critical review and a perspective on the outstanding issues. Nucleic Acid Ther 2017;27:251–259.
2. Emery AE. Population frequencies of inherited neuromuscular disease—a world survey. Neuromuscul Disord 1991;1:19–29.
3. Mendell JR, Lloyd-Puryear M. Report of MDA muscle disease symposium on newborn screening for Duchenne muscular dystrophy. Muscle Nerve 2013;48:21–26.
4. Mendell JR, Shilling C, Leslie ND, et al. Evidence based path to newborn screening for Duchenne muscular dystrophy. Ann Neurol 2012;71:304–313.
5. Oudet C, Hanauer A, Clemens P, et al. Two hot spots of recombination in the DMD gene correlate with the deletion prone regions. Hum Mol Genet 1992;1:599–603.
6. Brooke MH, Fenichel GM, Griggs RC, et al. Clinical investigation in Duchenne dystrophy: 2. Determination of the "power" of therapeutic trials based on the natural history. Muscle Nerve 1983;6:91–103.

7. Birnkrant DJ, Bushby K, Bann CM, et al. Diagnosis and management of Duchenne muscular dystrophy, part 1: diagnosis, and neuromuscular, rehabilitation, endocrine, and gastrointestinal and nutritional management. Lancet Neurol 2018;17: 251–267.

8. Liu D, Ahmet A, Ward L, et al. A practical guide to the monitoring and management of the complications of systemic corticosteroid therapy. Allergy Asthma Clin Immunol 2013;9:30.

9. Cirak S, Arechavala-Gomeza V, Guglier M, et al. Exon skipping and dystrophin restoration in patients with Duchenne muscular dystrophy after systemic phosphorodiamidate morpholino oligomer treatment: an open-label, phase 2, dose-escalation study. Lancet 2011;378:595–605.

10. Exondys 51 (eteplirsen) [prescribing information]. Cambridge, MA: Sarepta Therapeutics, Inc., 2018.

11. Mendell JR, Goemans N, Lowes LP, et al. Longitudinal effect of eteplirsen versus historical control on ambulation in Duchenne muscular dystrophy. Ann Neurol 2016;79:257–271.

12. Khan N, Eliopoulos H, Han L, et al. Eteplirsen treatment attenuates respiratory decline in ambulatory and non-ambulatory patients with Duchenne muscular dystrophy. J Neuromuscul Dis 2019;6:213–225.

13. Frank DE, Schnell FJ, Akana C, et al. Increased dystrophin production with golodirsen in patients with Duchenne muscular dystrophy. Neurology 2020;94:e2270–e2282.

14. Clemens PR, Rao VK, Connolly AM, et al. Safety, tolerability, and efficacy of viltolarsen in boys with Duchenne muscular dystrophy amenable to exon 53 skipping: a phase 2 randomized clinical trial. JAMA Neurol 2020;77:982–991.

15. Gregorevic P, Blankinship MJ, Allen JM, et al. Systemic microdystrophin gene delivery improves skeletal muscle structure and function in old dystrophic *mdx* mice. Mol Ther 2008;16:657–664.

16. Koo T, Okada T, Athanasopoulos T, et al. Long-term functional adeno-associated virus-microdystrophin expression in the dystrophic CXMDj dog. J Gene Med 2011;13:497–506.

17. Le Guiner C, Servais L, Montus M, et al. Long-term microdystrophin gene therapy is effective in a canine model of Duchenne muscular dystrophy. Nat Commun 2017;8:16105.

18. Liu M, Yue Y, Harper SQ, et al. Adeno-associated virus-mediated microdystrophin expression protects young *mdx* muscle from contraction-induced injury. Mol Ther 2005;11:245–256.

19. Shin JH, Pan X, Hakim CH, et al. Microdystrophin ameliorates muscular dystrophy in the canine model of duchenne muscular dystrophy. Mol Ther 2013;21:750–757.

20. Yue Y, Li Z, Harper SQ, et al. Microdystrophin gene therapy of cardiomyopathy restores dystrophin-glycoprotein complex and improves sarcolemma integrity in the *mdx* mouse heart. Circulation 2003;108:1626–1632.

21. Dongsheng D. Micro-dystrophin gene therapy goes systemic in Duchenne muscular dystrophy patients. Hum Gene Ther 2018;29:733–736.

22. Norwood FL, Sutherland-Smith AJ, Keep NH, et al. The structure of the N-terminal actin-binding domain of human dystrophin and how mutations in this domain may cause Duchenne or Becker muscular dystrophy. Structure 2000;8: 481–491.

23. Crawford GE, Faulkner JA, Crosbie RH, et al. Assembly of the dystrophin-associated protein complex does not require the dystrophin COOH-terminal domain. J Cell Biol 2000;150:1399–1410.

24. Koenig M, Kunkel LM. Detailed analysis of the repeat domain of dystrophin reveals four potential hinge segments that may confer flexibility. J Biol Chem 1990;265:4560–4566.

25. Suzuki A, Yoshida M, Yamamoto H, et al. Glycoprotein-binding site of dystrophin is confined to the cysteine-rich domain and the first half of the carboxy-terminal domain. FEBS Lett 1992;308: 154–160.

26. Jung D, Yang B, Meyer J, et al. Identification and characterization of the dystrophin anchoring site on beta-dystroglycan. J Biol Chem 1995;270: 27305–27310.

27. Harper SQ, Crawford RW, DelloRusso C, et al. Spectrin-like repeats from dystrophin and alpha-actinin-2 are not functionally interchangeable. Hum Mol Genet 2002;11:1807–1815.

28. Nelson DM, Lindsay A, Judge LM, et al. Variable rescue of microtubule and physiological phenotypes in *mdx* muscle expressing different miniaturized dystrophins. Hum Mol Genet 2018;27: 2090–2100.

29. Legardinier S, Hubert JF, Le Bihan O, et al. Subdomains of the dystrophin rod domain display contrasting lipid-binding and stability properties. Biochim Biophys Acta 2008;1784:672–682.

30. Zhao J, Kodippili K, Yue Y, et al. Dystrophin contains multiple independent membrane-binding domains. Hum Mol Genet 2016;25:3647–3653.

31. Rodino-Klapac LR, Janssen PM, Montgomery CL, et al. A translational approach for limb vascular delivery of the micro-dystrophin gene without high volume or high pressure for treatment of Duchenne muscular dystrophy. J Transl Med 2007;5: 45.

32. Salva MZ, Himeda CL, Tai PW, et al. Design of tissue-specific regulatory cassettes for high-level rAAV-mediated expression in skeletal and cardiac muscle. Mol Ther 2007;15:320–329.

33. Rodino-Klapac LR, Janssen PM, Shontz KM, et al. Micro-dystrophin and follistatin co-delivery restores muscle function in aged DMD model. Hum Mol Genet 2013;22:4929–4937.

34. Rodino-Klapac LR, Montgomery CL, Bremer WG, et al. Persistent expression of FLAG-tagged micro dystrophin in nonhuman primates following intramuscular and vascular delivery. Mol Ther 2010; 18:109–117.

35. Harper SQ, Hauser MA, DelloRusso C, et al. Modular flexibility of dystrophin: implications for gene therapy of Duchenne muscular dystrophy. Nat Med 2002;8:253–261.

36. Sondergaard P, Griffin D, Pozsgai E, et al. AAV .dysferlin overlap vectors restore function in dysferlinopathy animal models. Ann Clin Transl Neurol 2015;2:256–270.

37. Mendell JR, Rodino-Klapac LR, Rosales XQ, et al. Sustained alpha-sarcoglycan gene expression after gene transfer in limb-girdle muscular dystrophy, type 2D. Ann Neurol 2010;68:629–638.

38. Schnepp BC, Jensen RL, Chen CL, et al. Characterization of adeno-associated virus genomes isolated from human tissues. J Virol 2005;79: 14793–14803.

39. Pozsgai ER, Griffin DA, Heller KN, et al. Systemic AAV-mediated β-sarcoglycan delivery targeting cardiac and skeletal muscle ameliorates histological and functional deficits in LGMD2E mice. Mol Ther 2017;25:855–869.

40. Beastrom N, Lu H, Macke A, et al. *mdx*^{5cv} mice manifest more severe muscle dysfunction and diaphragm force deficits than do *mdx* Mice. Am J Pathol 2011;179:2464–2474.

41. Rafael-Fortney JA, Chimanji NS, Schill KE, et al. Early treatment with lisinopril and spironolactone preserves cardiac and skeletal muscle in Duchenne muscular dystrophy mice. Circulation 2011;124:582–588.

42. Moorwood C, Liu M, Tian Z, et al. Isometric and eccentric force generation assessment of skeletal muscles isolated from murine models of muscular dystrophies. J Vis Exp 2013;71:e50036.

43. Heller KN, Montgomery CL, Shontz KM, et al. Human α7 integrin gene (*ITGA7*) delivered by adeno-associated virus extends survival of severely affected dystrophin/utrophin-deficient mice. Hum Gene Ther 2015;26:647–656.

44. Hakim CH, Li D, Duan D. Monitoring murine skeletal muscle function for muscle gene therapy. Methods Mol Biol 2011;709:75–89.

45. Clark KR, Liu X, McGrath JP, et al. Highly purified recombinant adeno-associated virus vectors are biologically active and free of detectable helper and wild-type viruses. Hum Gene Ther 1999;10: 1031–1039.

46. Pozsgai ER, Griffin DA, Heller KN, et al. Beta-sarcoglycan gene transfer decreases fibrosis and restores force in LGMD2E mice. Gene Ther 2016; 23:57–66.

47. Glen BB, Luke MJ, James MA, et al. The polyproline site in hinge 2 influences the functional capacity of truncated dystrophins. PLoS Genet 2010;6:e1000958.

48. Ramos JN, Hollinger K, Bengtsson NE, et al. - Development of novel micro-dystrophins with enhanced functionality. Mol Ther 2019;27:623–635.

49. Adams ME, Odom GL, Kim MJ, et al. Syntrophin binds directly to multiple spectrin-like repeats in

dystrophin and mediates binding of nNOS to repeats 16–17. Hum Mol Genet 2018;27:2978–2985.

50. Lai Y, Zhao J, Yue Y, et al. α2 and α3 helices of dystrophin R16 and R17 frame a microdomain in the α1 helix of dystrophin R17 for neuronal NOS binding. Proc Natl Acad Sci U S A 2012;110:525–530.
51. Chicoine LG, Montgomery CL, Bremer WG, et al. Plasmapheresis eliminates the negative impact of AAV antibodies on microdystrophin gene expression following vascular delivery. Mol Ther 2014; 22:338–347.
52. Chicoine LG, Rodino-Klapac LR, Shao G, et al. Vascular delivery of rAAVrh74.MCK.GALGT2 to the gastrocnemius muscle of the rhesus macaque stimulates the expression of dystrophin and laminin α2 surrogates. Mol Ther 2014;22:713–724.
53. Xu R, Jia Y, Zygmunt DA, et al. An isolated limb infusion method allows for broad distribution of rAAVrh74.MCK.GALGT2 to leg skeletal muscles in the rhesus macaque. Mol Ther Methods Clin Dev 2018;10:89–104.
54. Mendell JR, Sahenk Z, Lehman K, et al. Assessment of systemic delivery of rAAVrh74.MHCK7 .micro-dystrophin in children with Duchenne muscular dystrophy: A nonrandomized trial. JAMA Neurol 2020;77:1122–1131.
55. Zygmunt DA, Crowe KE, Flanigan KM, et al. Comparison of serum rAAV serotype-specific antibodies in patients with Duchenne muscular dystrophy, Becker muscular dystrophy, inclusion body myositis, or GNE myopathy. Hum Gene Ther 2017;28:737–746.
56. Duan D. Systemic AAV micro-dystrophin gene therapy for Duchenne muscular dystrophy. Mol Ther 2018;26:2337–2356.
57. Yoshimura M, Sakamoto M, Ikemoto M, et al. AAV vector-mediated microdystrophin expression in a relatively small percentage of *mdx* myofibers improved the *mdx* phenotype. Mol Ther 2004;10: 821–828.
58. Banks GB, Judge LM, Allen JM, et al. The polyproline site in hinge 2 influences the functional capacity of truncated dystrophins. PLoS Genet 2010;6:e1000958.
59. Mendell JR, Campbell K, Rodino-Klapac L, et al. Dystrophin immunity in Duchenne's muscular dystrophy. N Engl J Med 2010;363:1429–1437.
60. Talsness DM, Belanto JJ, Ervasti JM. Disease-proportional proteasomal degradation of missense dystrophins. Proc Natl Acad Sci U S A 2015;112: 12414–12419.
61. McCourt JL, Rhett KK, Jaeger MA, et al. In vitro stability of therapeutically relevant, internally truncated dystrophins. Skelet Muscle 2015;28:13.
62. Gao QQ, McNally EM. The dystrophin complex: structure, function, and implications for therapy. Compr Physiol 2015;5:1223–1239.
63. Lai Y, Thomas GD, Yue Y, et al. Dystrophins carrying spectrin-like repeats 16 and 17 anchor nNOS to the sarcolemma and enhance exercise performance in a mouse model of muscular dystrophy. J Clin Invest 2009;119:624–635.
64. Hakim CH, Wasala NB, Pan X, et al. A five-repeat micro-dystrophin gene ameliorated dystrophic phenotype in the severe DBA/2J-*mdx* model of Duchenne muscular dystrophy. Mol Ther Methods Clin Dev 2017;6:216–230.
65. Yue Y, Pan X, Hakim CH, et al. Safe and bodywide muscle transduction in young adult Duchenne muscular dystrophy dogs with adeno-associated virus. Hum Mol Genet 2015;24:5880–5890.
66. Percival JM, Anderson KN, Huang P, et al. Golgi and sarcolemmal neuronal NOS differentially regulate contraction-induced fatigue and vasoconstriction in exercising mouse skeletal muscle. J Clin Invest 2010;120:816–826.
67. Rebolledo DL, Kim MJ, Whitehead NP, et al. Sarcolemmal targeting of nNOSμ improves contractile function of *mdx* muscle. Hum Mol Genet 2016;25:158–166.
68. Crosbie RH, Straub V, Yun HY, et al. *mdx* muscle pathology is independent of nNOS perturbation. Hum Mol Genet 1998;7:823–829.
69. Chao DS, Silvagno F, Bredt DS. Muscular dystrophy in *mdx* mice despite lack of neuronal nitric oxide synthase. J Neurochem 1998;71:784–789.

Received for publication September 17, 2020
accepted after revision November 24, 2020

Published online: January 4, 2021